BIOCHEMISTRY

 Volume 44, Number 29 July 26, 2005

Articles

Thermostable Direct Hemolysin of *Vibrio parahaemolyticus* Is a Bacterial Reversible Amyloid Toxin†

Takashi Fukui,‡ Kentaro Shiraki,§ Daizo Hamada,‡ Kojiro Hara,|| Tomoko Miyata,⊥ Shinsuke Fujiwara,#,+ Kouta Mayanagi,⊥ Keiko Yanagihara,‡ Tetsuya Iida,|| Eiichiro Fukusaki,# Tadayuki Imanaka,@ Takeshi Honda,|| and Itaru Yanagihara*,‡

Department of Developmental Infectious Diseases, Research Institute, Osaka Medical Center for Maternal and Child Health, 840 Murodo-cho, Izumi, Osaka 594-1101, Japan, Institute of Applied Physics, University of Tsukuba, 1-1-1 Tennodai, Tsukuba, Ibaraki 305-8573, Japan, Department of Biotechnology, Graduate School of Engineering, Osaka University, 2-1 Yamadaoka, Suita, Osaka 565-0871, Japan, Department of Bacterial Infections, Research Institute for Microbial Diseases, Osaka University, 3-1 Yamadaoka, Suita, Osaka 565-0871, Japan, Biomolecular Engineering Research Institute, 6-2-3 Furuedai, Suita, Osaka 565-0874, Japan, and Department of Synthetic Chemistry and Biological Chemistry, Graduate School of Engineering, Kyoto University, Katsura, Nishikyo-ku, Kyoto 615-8510, Japan

Received February 20, 2005; Revised Manuscript Received May 31, 2005

ABSTRACT: Thermostable direct hemolysin (TDH), a major virulence factor of *Vibrio parahaemolyticus*, is detoxified by heating at ~60−70 °C but is reactivated by additional heating above 80 °C. This paradoxical phenomenon, known as the Arrhenius effect, has remained unexplained for ~100 years. We now demonstrate that the effect is related to structural changes in the protein that produce fibrils. The native TDH (TDHn) is transformed into nontoxic fibrils rich in β-strands by incubation at 60 °C (TDHi). The TDHi fibrils are dissociated into unfolded states by further heating above 80 °C (TDHu). Rapid cooling of TDHu results in refolding of the protein into toxic TDHn, whereas the protein is trapped in the TDHi structure by slow cooling of TDHu. Transmission electron microscopy indicates the fibrillar structures of TDHi. The fibrils show both the property of the nucleation-dependent elongation and the increase in its thioflavin T fluorescence. Formation of β-rich structures of TDH was also observed in the presence of lipid vesicles containing ganglioside G_{T1b}, a putative TDH receptor. Congo red was found to inhibit the hemolytic activity of TDH in a dose-dependent manner. These data reveal that the mechanism of the Arrhenius effect which is tightly related to the fibrillogenicity of TDH.

Vibrio parahaemolyticus is a Gram-negative rod-shaped marine bacterium that is a common cause of food-borne gastroenteritis. A major virulence factor of this pathogen is thermostable direct hemolysin (TDH).[1] The hemolytic activity of TDH is inactivated by heating at 60 °C but is

† This work was supported by the MEXT, a Grant-in-Aid for Scientific Research in Priority Areas (I.Y. and D.H.); Japan Food Industry Center (I.Y. and E.F.); JSPS, through a Research Fellowship for Young Scientists (D.H.); CREST, Japan (T.I.); and Research for the Future Program (T.H.).

* To whom correspondence should be addressed. Telephone: +81-725-56-1220. Fax: +81-725-57-3021. E-mail: itaruy@mch.pref.osaka.jp.

‡ Osaka Medical Center for Maternal and Child Health.

§ University of Tsukuba.

|| Research Institute for Microbial Diseases, Osaka University.

⊥ Biomolecular Engineering Research Institute.

Graduate School of Engineering, Osaka University.

+ Present address: Department of Bioscience, School of Science and Technology, Kwansei Gakuin University, 2-1 Gakuen, Sanda 669-1337, Japan.

@ Kyoto University.

10.1021/bi050311s CCC: $30.25
Published on Web 06/30/2005

unaffected by heating for 15 min at 100 °C (*1*). There are several bacterial toxins which show such paradoxical responses to heat treatment, known as the Arrhenius effect since the early 1900s: α-hemolysin of *Staphylococcus aureus* (*2*), exotoxin of *Pseudomonas aeruginosa* (*3*), hemolysins of *Bacillus cereus* (*4*) and *Klebsiella pneumoniae* (*5*), and TDH. Although the Arrhenius effect has been recognized for ~100 years, the underlying molecular mechanism remains unclear.

TDH is composed of 165 amino acids and has a single intramolecular disulfide bond (*6*). TDH binds ganglioside G_{T1b} (*7*), a putative TDH receptor, found in neuronal cell membranes and endoplasmic reticulum. Hemolytic activity assays with various colloidal compounds, as well as electron microscopic observations of freeze-fractured preparations, show the presence of porelike structures on the surface of membranes treated with TDH (*8*). Although other bacterial pore-forming toxins are known to form ordered oligomeric structures on the surface of the membrane (*9*−*12*), the detailed oligomerized pore-forming structure of TDH has not been identified. Expression of green fluorescence protein (GFP)−TDH fusion proteins in Rat-1 cultured cells shows that TDH causes apoptosis (*13*). These data indicate that TDH is toxic both inside and outside the cultured cells, although the precise mechanism of TDH-induced membrane damage has not yet been clarified.

Some proteins and peptide fragments are prone to forming amyloid fibrils and cause specific diseases, including Alzheimer's disease, amyloidosis, and prion-caused neurodegenerative disorders such as Creutzfeldt-Jakob disease and bovine spongiform encephalopathy (*14*). However, several proteins and synthetic polypeptides are not implicated in specific diseases but can associate into fibrillar aggregates in vitro under carefully chosen conditions (*15*−*20*). To date, more than 20 proteins are known to form amyloid fibrils either in vitro or in vivo. Although no conserved sequences among the amyloidogenic proteins have been found, it has been proposed that the amyloidogenicity of polypeptide chains is largely associated with simple physicochemical parameters (*21*, *22*). The amyloid fibril consists of cross-β structures that tend to be more stable than the native form (*23*−*25*). These fibrils are formed either heterodimerically (*26*) or by nucleation-dependent polymerization, also known as the seeding effect, around multiple sites in the nucleus, resulting in rapid polymerization and growth (*27*).

In this study, we analyzed the structure of TDH by several spectroscopic and electron microscopic techniques under various heat treatments. Below 50 °C, TDH exists in oligomeric native states that consist predominantly of β-sheet structures. When heated to ~60 °C, TDH is transformed into fibrillar aggregates rich in β-strands. These fibrils are stable even when the heated TDH sample is returned to low temperatures. The TDH fibrils do not show native hemolytic activity at 37 °C. However, irrespective of whether TDH is in the form of fibrils or the native structure prior to being heated, once the protein is heated at 90 °C it becomes fully unfolded. Furthermore, the heat-induced unfolded TDH refolds into the native toxic form when it is rapidly cooled to 37 °C. These results clarify the mechanism of the Arrhenius effect. TDH is detoxified by aggregation into fibrils after being heated at 60−70 °C, which can be reversibly refolded into the toxic native form by being rapidly cooled after unfolding at higher temperatures.

We also show that a conformational state having β-strands, possibly similar to those of fibrillar TDH, is stabilized when the protein is bound to several different lipid membranes. The hemolytic activity of TDH is suppressed by the addition of Congo red, a dye known to be sensitive to amyloid fibrils. These findings support the idea that the conformational change in TDH, with the increase in β-sheet content, in a cellular membrane, may be associated with its cytotoxicity.

EXPERIMENTAL PROCEDURES

Proteins and Hemolytic Activity. Plasmid vector pKK223-3, harboring wild-type *tdh* or mutant *r7* genes for TDH (G62S), was transformed into *Escherichia coli* JM 109 cells. Recombinant TDH and R7 were purified by hydroxyapatite, anion-exchange, and gel filtration chromatography (*13*). Hemolytic activity was assayed according to a previously described method (*28*) with rabbit red blood cells (rRBC) (Nippon Bio-Test Laboratories, Tokyo, Japan). For size-exclusion analysis, 0.1 mg of native or heat-treated TDH was applied to a Superose 6 HR column using an ÄKTA explorer 10S instrument (Amersham-Pharmacia, Uppsala, Sweden).

CD Spectrum. Circular dichroism (CD) spectra were recorded with a J-720W spectropolarimeter (JASCO, Tokyo, Japan) equipped with a thermoelectric temperature controller. Data were processed with software provided by JASCO. Measurements were taken in a quartz cuvette with a path length of 2 mm, scanned in steps of 0.2 nm at a rate of 50 nm/min. The data from 5 to 20 runs were averaged. The protein concentrations were 0.18 and 0.36 mg/mL for measurements of far- and near-UV CD spectra, respectively.

The heat-induced conformational transitions of TDH were evaluated by the ellipticity at 212 nm. Samples of 0.09 mg/mL TDH in 10 mM phosphate buffer (PB) at pH 7.4 were heated from 37 to 95 °C at a heating rate of 0.1 °C/min. To determine the differences in structure with different cooling treatments, the temperature was decreased rapidly (30 °C/min) or slowly (1 °C/min) from 95 to 37 °C. The experiments were repeated twice to evaluate the reproducibility.

Electron Microscope Observations. Solutions containing 0.13 mg/mL TDH in different conformational states were diluted with 10 mM PB at pH 7.0. For negative staining, 4 μL of the sample solution was applied to a copper grid supporting a continuous thin-carbon film, left for 1 min, and then stained with 3 drops of 2% uranyl acetate. Images were recorded at a magnification of 70 000 times on FG film (Fuji photo film, Tokyo, Japan) using a 100CX electron microscope (JEOL, Tokyo, Japan). Images were saved on a disk after scanning with a CCD scanner.

Fourier Transform Infrared Spectroscopy (FT-IR). Infrared spectra were recorded using an AVATAR370 FT-IR spectrometer (Thermo Nicolet Co., Madison, WI) under a continuous purge with dry nitrogen gas. The nominal spectral resolution was 2 cm^{-1}. Spectra of 128 scans were averaged.

[1] Abbreviations: TDH, thermostable direct hemolysin; TDHn, native TDH; TDHi, intermediate of TDH with fibrillar structure; TDHu, unfolded TDH; CD, circular dichroism; FT-IR, Fourier transform infrared spectroscopy; rRBC, rabbit red blood cells; DMPG, dimyristoylphosphatidylglycerol; PB, phosphate buffer; PBS, phosphate-buffered saline; Aβ, amyloid β; β_2-m, β_2-microglobulin.

A Happ−Genzel apodization function was applied before Fourier transformation. The native TDH in H_2O was lyophilized and subsequently dissolved in 10 mM sodium phosphate and ^2H_2O at p^{2}H 7.4 (pH meter reading without correcting for the isotope effect). The fibrils of TDH were prepared by heat treatment at 60 °C, and the aggregates were collected by centrifugation. The precipitates were washed twice with 10 mM sodium phosphate and ^2H_2O at p^{2}H 7.4 and resuspended in the same buffer. The TDH solutions were transferred to an IR sample cell consisting of a pair of CaF_2 windows separated by a 15 μm spacer. FT-IR measurements were carried out at room temperature.

Thioflavin T Assay for Fibrillation. The fluorescence of thioflavin T was measured at 460−570 nm with an excitation wavelength of 450 nm using a T-2000 (Hitachi High-technologies Co., Tokyo, Japan) (Figure 5A) or FP-6500 (JASCO) (Figure 6) fluorescence spectrophotometer. Protein solutions were incubated with 5 μM thioflavin T (Sigma-Aldrich, Inc., St. Louis, MO) in 50 mM glycine-NaOH (pH 8.5).

Kinetics of Formation of Fibrils by TDH. Protein solutions of 0.35 mg/mL in 10 mM PB at pH 7.4 were prepared in 1.5 mL plastic tubes with lids. For seeding experiments, 5% (v/v) aliquots of the solution containing preformed fibrils were added to the TDHn solution prior to incubation. The mixture was incubated at 45 °C. TDHi used for seeding was prepared by sonication of elongated fibrils formed by heating the TDH solution in a bath-type sonicator (Bioruptor UCD-200TM, Tosho Electronics Ltd., Tokyo, Japan) for 15 min. At each incubation time, a 5 μL aliquot of the solution was withdrawn and then mixed with 400 μL of the thioflavin T solution.

Each kinetic trace was fitted to the stretched exponential function $F = F_\infty + \Delta F \exp[-(kt)^n]$, where k is the rate constant (per hour), n is the heterogeneity parameter, F and F_∞ are the fluorescence intensity (arbitrary units) at a given time and at the end of the reaction, respectively, and ΔF is the amplitude of the reaction (arbitrary units per hour) (*20*).

Preparation of Lipid Vesicles. Total lipids and glycolipids from rRBC, the acidic lipid dimyristoylphosphatidylglycerol (DMPG) (Sigma-Aldrich), bovine brain ganglioside mixture (G. mix) (Sigma-Aldrich), and ganglioside G_{T1b} (Sigma-Aldrich) were extracted with a 1:1 chloroform/methanol mixture. The organic fraction was completely dried in a rotary evaporator, and the dried lipids were resuspended in phosphate-buffered saline (PBS) to a concentration of 1 mg/mL. Repeated ultrasonic and vortex treatments were applied to prepare the lipid vesicles (*29*, *30*). For CD spectroscopy, lipid vesicles (100 μL) were then mixed with 300 μL of PBS containing TDH at a final concentration of 0.05 mg/mL.

Inhibitory Effect of Congo Red on Hemolysis. Various concentrations of Congo red were preincubated with 5 μg of TDH for 30 min at 4 °C. The TDH solution, with or without Congo red, was incubated with 4% rabbit red blood cells (Nippon Bio-supply Center, Tokyo, Japan) in a total volume of 200 μL for 30 min at 37 °C. To exclude the remaining Congo red, samples were washed three times in PBS and the intact red blood cells were collected by gentle centrifugation. Complete hemolysis was achieved by the addition of 2 μL of polyoxyethylene (*10*) octylphenyl ether. Hemolytic activities were calculated from the UV spectrum as described previously (*28*).

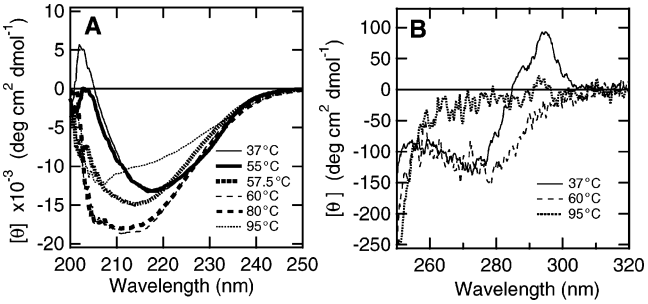

FIGURE 1: Far-UV (A) and near-UV (B) CD spectra of TDH in 10 mM PB (pH 7.4) at 37 (solid line), 55 (thick solid line), 57.5 (thick dotted line), 60 (dashed line), 80 (thick dashed line) and 95 °C (dotted line).

RESULTS

Heat-Induced Conformational Changes in TDH. The far-UV CD spectra of native TDH (TDHn) in 10 mM PB (pH 7.4) below 55 °C exhibited a minimum at 218 nm (Figure 1A), suggesting that the protein consists predominantly of β-sheet structures. The absolute ellipticity in the far-UV region increased upon incubation at 60−80 °C, whereas the value decreased by further increasing the temperature to 95 °C. The spectra obtained at 60−80 °C have a minimum ellipticity between −15000 and −20000 deg cm^2 dmol^{-1} at 212−215 nm. This suggests an increased β-sheet content compared with that of the native structure formed at lower temperatures. However, the spectrum obtained at 80 °C was typical of an unfolded polypeptide. This result suggests at least three states are responsible for the heat-induced transitions shown by TDH: a native state (TDHn) below 55 °C, an intermediate state (TDHi) at 60−80 °C, and a fully unfolded state (TDHu) above 80 °C.

The near-UV CD spectrum of TDHn exhibited a negative peak at 275 nm, and positive peaks at 288 and 295 nm (Figure 1B), indicating that TDHn has specific tertiary structures. At 60 °C, however, the peaks at 295 and 288 nm disappeared, and only the peak at 275 nm was observed. This suggested that TDHi has a particular ordered conformation that may include tertiary contacts similar to those of TDHn. The spectrum at 95 °C indicates no obvious peaks, which is consistent with the formation of a fully unfolded structure of TDHu drawn from far-UV CD data.

The Arrhenius Effect Can Be Rationalized by the Conformational Changes of TDH. CD analysis showed that TDH could interconvert among at least three conformational states (TDHn, TDHi, and TDHu), depending on the temperature. This property of TDH can potentially explain the mechanism underlying the Arrhenius effect. However, the hemolytic activity of TDH is normally tested at 37 °C. Unless it is trapped as an irreversible aggregate, conformational changes occur with variations in temperature. To check the reversibility of the heat-induced transitions of TDH, we monitored the temperature dependence of the ellipticity at 212 nm by heating at a rate of 0.1 °C/min [Figure 2A (□)].

When the TDH solution was heated, the absolute ellipticity at 212 nm increased in the range of 60−70 °C, but then gradually decreased to the value of the unfolded state above 70 °C. These data suggest that heating induces a conformational change from TDHn to an unfolded state, TDHu, via TDHi. To examine the effect of the cooling rate on the secondary structure of TDH, we controlled the temperature

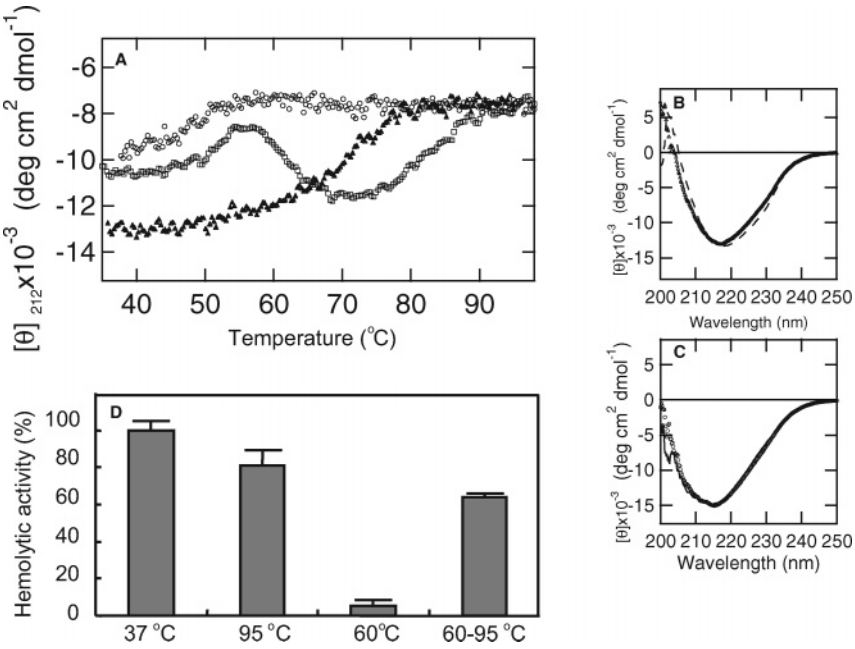

FIGURE 2: Effect of heat treatment on the conformation of TDH. (A) Thermal unfolding and refolding profile of TDH monitored by the ellipticity at 212 nm [slow heating at 0.1 °C/min (□), rapid cooling at 30 °C/min (○), and slow cooling at 1 °C/min (▲)]. (B) CD spectrum of TDH at 37 °C after rapid cooling (△). The spectrum is identical to that of TDHn (dashed line). (C) CD spectrum of TDH at 37 °C after slow cooling (○). The spectrum was identical to that of TDHi at 57.5 °C (solid line). (D) Relative hemolytic activities of TDH, measured at 37 °C after various heat treatments ($n = 5$ per group).

decrease from 95 °C where TDH assumes the unfolded state. At a cooling rate of 1 °C/min, the absolute ellipticity increased to the value for TDHi until the temperature fell to less than 75 °C. However, the intensity did not recover to the value for TDHn even at lower temperatures [Figure 2A (▲)]. When the solution was slowly cooled, the CD spectrum of TDH at 37 °C was identical to that of TDHi at 57.5 °C (Figure 2C). This indicates that, at least within the time range of the experiment, the protein is trapped in the TDHi conformation even at low temperatures where normally TDHn should have accumulated. Conversely, TDH that initially unfolded at high temperatures can be renatured by being rapidly cooled at a rate of 30 °C/min [Figure 2A (○)]. Thus, in this case the reaction is reversible. The reversibility of the reaction was also confirmed by the observation that the peak at 218 nm in the far-UV CD spectrum reappeared after rapid cooling of heat-unfolded TDH (Figure 2B). These findings indicate that not only the thermal environment but also the rate of cooling influences the structural changes of TDH.

Interestingly, the hemolytic activity of TDH on rabbit red blood cells was consistent with the conformational property of this protein at 37 °C after different heat treatments (Figure 2D). The hemolytic activity of unheated TDH, i.e., TDHn, (3 μg/mL) at 37 °C was designated as 100% hemolysis (Figure 2D, column 1, 37 °C). Incubation of the protein at 95 °C for 15 min followed by rapid cooling (30 °C/min) to 37 °C gave a hemolytic activity of 80.8 ± 8.4% (mean ± standard deviation, Figure 2D, column 2, 95 °C). Incubation of the protein at 60 °C for 15 min followed by slow cooling (1 °C/min) to 37 °C gave a hemolytic activity of only 5.5 ± 2.9% (Figure 2D, column 3, 60 °C). Next, we inactivated TDH at 60 °C for 15 min before further heating the sample to 95 °C. After a 15 min incubation at 95 °C, the sample was rapidly cooled to 37 °C (30 °C/min). TDH subjected to this treatment recovered its hemolytic activity: 63.7 ± 1.5% (Figure 2D, column 4, 60−95 °C).

Thus, the paradoxical inactivation phenomenon of TDH, known as the Arrhenius effect, is due to a conformational trap at the TDHi structure formed by a particular heating and cooling regimen. The trapped structure can be readily recovered by heating the protein above 80 °C and rapidly cooling it to a much lower temperature.

Characterization of TDHi. The data from the CD spectra indicate that TDH undergoes changes in conformation depending on the temperature. This conformational change in TDH is directly related to its cytotoxic ability. To understand the nature of TDHi, a nontoxic form of this protein, we further analyzed its conformational properties.

Molecular Organization of TDHi. Gel filtration analysis of TDHi showed it to elute in the void volume, indicating a molecular mass of >440 kDa (Figure 3A). In contrast, TDHn gave an estimated molecular mass of approximately 65 kDa by this technique. The molecular mass of the TDH monomer calculated from its amino acid sequence is 18.6 kDa. Hence, assuming the molecule behaves as a globular protein, TDHn appears to exist as either a trimer or tetramer in 10 mM PB, whereas TDHi exists in a large oligomeric state.

The detailed structure of the large oligomeric state of TDHi (Figure 3C−E) was observed by transmission electron microscopy. The image of TDHi indicates the presence of fibrillar structures, which are distinct from nonspecific amorphous aggregates usually formed by proteins after heat treatment. The image of TDHn (Figure 3B) indicates the presence of ringlike structures, probably formed by the association of globular proteins.

Interestingly, the fibrils of TDHi lengthened over time (self-elongation), as shown previously for amyloid fibrils of other proteins (*27*). TDHi, prepared by heating at 60 °C for 15 min followed by slow cooling (1 °C/min) to 4 °C, was

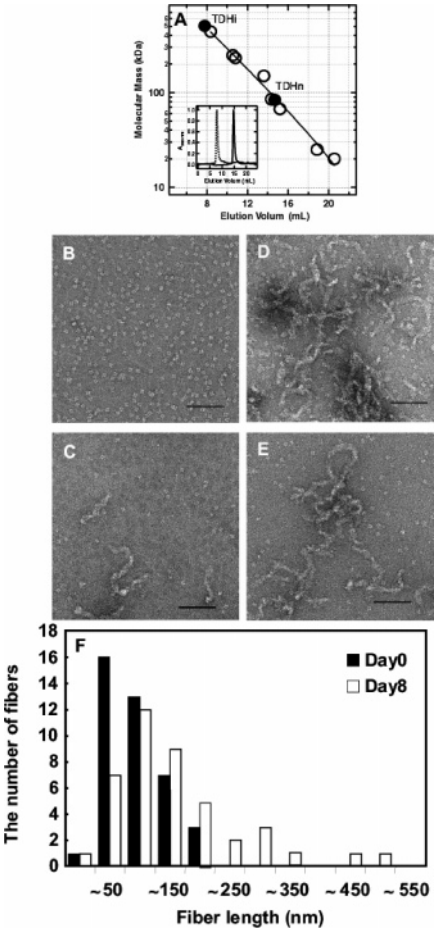

FIGURE 3: Structure of oligomeric TDHi. (A) Estimated molecular mass of TDHi and TDHn. The inset shows the gel filtration analysis of TDHn (solid line) and TDHi (dotted line). White circles indicate molecular mass standards: 440 kDa, ferritin; 247 kDa, phenylalanyl-tRNA synthetase from *Thermococcus kodakaraencis* KOD1; 232 kDa, catalase; 150 kDa, aldolase; 67 kDa, albumin; 25 kDa, chymotrypsinogen A; and 20 kDa, O^6-methylguanine-DNA methyltransferase from *T. kodakaraencis* KOD1. (B−F). Electron micrographs of various TDH structures. TDHn (B). Spontaneous elongation at 4 °C of TDH seeded with heat-treated TDHi: days 0 (C), 1 (D), and 8 (E). The bar is 60 nm. (F) Histogram of TDHi fiber length observed on days 0 and 8.

incubated for up to 8 days at 4 °C (Figure 3C−E). The TDHi images showed the fibrils to have a diameter of 7−10 nm and a length of 100 to >200 nm (Figure 3C−E). The length of the TDHi fibrils at 4 °C was measured on days 0 and 8 (Figure 3F). The mean fibril length on day 0, just after heat treatment, was 119.3 ± 49.2 nm (n = 40; minimum length of 43.7 nm; maximum length of 234.1 nm), while on day 8, the fibrils had elongated to 181.4 ± 108.1 nm (n = 42; minimum length of 46.9 nm; maximum length of 507.7 nm). In the absence of heat treatment, TDH exhibited no such conformational transition even after 8 days at 4 °C (data not shown).

FT-IR. FT-IR spectroscopy is ideal for determining the secondary structure of polypeptide chains, particularly when they associate into large aggregates. The amide I′ band, in the wavenumber region from 1600 to 1700 cm^{-1}, is useful since the band frequencies are characteristic of different secondary structural elements.

Characteristic peaks around 1640−1620 cm^{-1} for TDHn and TDHi indicate the formation of β-strand structures.

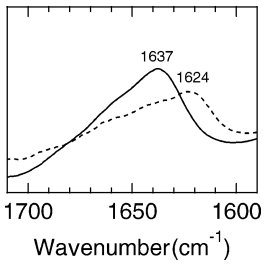

FIGURE 4: FT-IR spectra of TDHn (solid line) and TDHi (dashed line) in ^2H_2O at p^{2}H 7.4.

However, the spectrum for TDHi differs significantly from that of TDHn (Figure 4) and contains a high-frequency, high-intensity band at 1624 cm^{-1}. The position of this band is characteristic of intermolecular antiparallel β-sheets, as observed for various aggregated proteins.

Thioflavin T Assay. The fluorescence intensity of thioflavin T increases when it binds to amyloid fibrils (*31*). Interestingly, the thioflavin T fluorescence in the presence of TDHi was ~100 times greater than with TDHn (Figure 5A). This suggests the presence of cross-β structures in TDHi and is consistent with the CD and FT-IR spectra that also indicate the presence of β-sheet structures. TDHn and TDHu exhibited no such increase in fluorescence intensity after incubation with thioflavin T (Figure 5A).

The R7 mutant of TDH, in which serine replaces glycine at position 62, lacks hemolytic activity (*28*). R7 after heat treatment at 60 °C for 15 min exhibited less intense thioflavin T fluorescence than TDHi (Figure 5A). Fibril formation is correlated to the hemolytic activity of TDH (discussed in detail below).

Seeding Experiments. It is well established that the rate of formation of fibrils by amyloidogenic proteins is promoted by the addition of preformed fibrils (seeding effect). The kinetics of fibril formation was monitored by the intensity of thioflavin T fluorescence. In the absence of seed, the increase in the intensity of thioflavin T fluorescence occurs only after a lag phase of 6−12 h. In contrast, in the presence of seed, the rate of the increase in fluorescence intensity was much enhanced (Figure 6).

The results shown in Figure 6 are consistent with the model of nucleation-dependent elongation of fibrils. Such reaction kinetics can be empirically fitted to the stretched exponential function $F = F_\infty + \Delta F \exp[-(kt)^n]$ (see Experimental Procedures). According to this equation, when the n value is equal to 1, the curve can be expressed by a single-exponential function with a rate constant of k. When $0 < n < 1$, the kinetics can be approximated by a multiexponential function indicative of multiple events. However if $n > 1$, the curves represent a sigmoidal transition with an initial lag phase, as shown for the reaction kinetics in the absence of seed (*20*). The kinetic parameters F_∞, ΔF, k, and n of the seeded condition were 186.0, 156.0, 0.01 h^{-1}, and 1.0, respectively (fluorescence intensity in arbitrary units). When the same F_∞ value was used for fitting, ΔF, k, and n for the unseeded condition were 180.8, 0.005 h^{-1}, and 1.15, respectively. Thus, the kinetic trace of fibril growth under unseeded conditions contains a lag phase with a lower rate constant, which is half that for the seeded condition.

CD Spectrum of TDH in the Presence of Lipid Vesicles. The finding that the heat-aggregated R7 mutant shows a

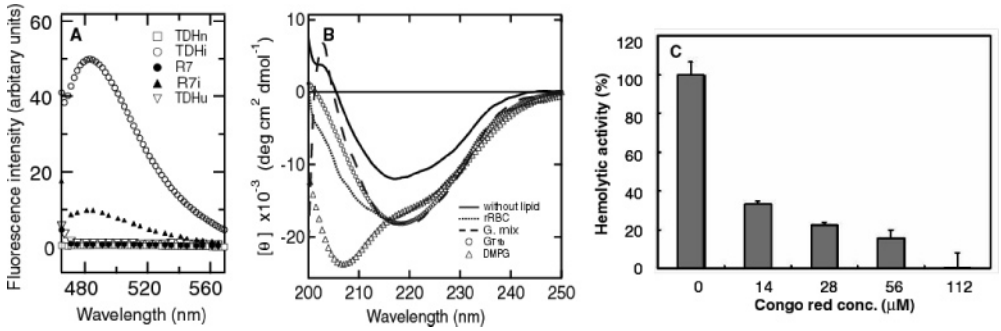

FIGURE 5: Fibrillogenic ability vs hemolytic activity of TDH. (A) Thioflavin T fluorescence in the presence of TDHn (□), TDHi (○), TDHu (▽), R7 (●), and R7i (▲). (B) Far-UV CD spectra of TDH in the presence of various lipid vesicles. (C) Inhibitory effect of Congo red (0, 14, 28, 56, and 112 μM) on TDH hemolysis ($n = 4$ per group).

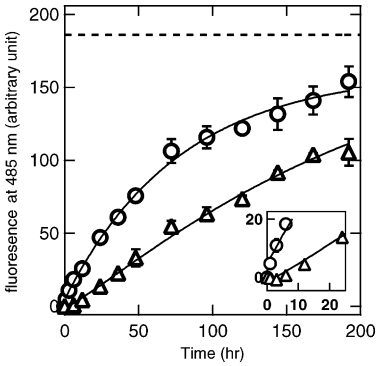

FIGURE 6: Seeding effect of TDH fibril formation with preformed TDHi fibrils. The solutions were incubated at 45 °C with or without added 5% (v/v) aliquots of a solution containing preformed fibrils, not seeded (△) or seeded with preformed TDHi (○). The dotted line indicates F_∞ determined by fitting the kinetics in the presence of seed. The inset shows the lag phase for the unseeded solution (from 0 to 24 h).

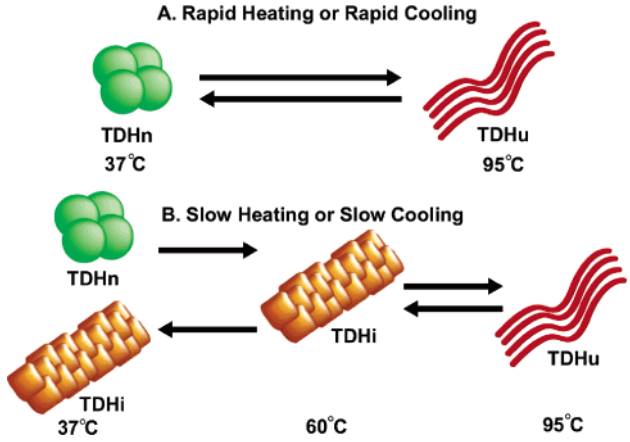

FIGURE 7: Model of heat-induced conformational change of TDH. Rapid heating and cooling (A). Slow heating and cooling (B).

lower intensity of thioflavin T fluorescence suggests that R7 is less prone to forming fibrillar structures than wild-type TDH. This implies that the hemolytic activity of TDH may be related to its tendency to form fibrillar aggregates. In this sense, it is interesting to analyze the conformational property of TDH when it is bound to a lipid bilayer, which mimics the biological membrane. We, therefore, measured the far-UV CD spectra for TDH in the presence of various lipid vesicles.

As previously shown for several other polypeptides (*32*), the CD spectrum of TDH changed into that characteristic of α-helical structures in the presence of DMPG lipid vesicles (Figure 5B). However, the spectra of TDH in the presence of vesicles containing gangliosides (Figure 5B, rRBC, G. mix, G_{T1b}) are similar to that of heat-treated TDHi (Figure 1A). These results are consistent with an earlier observation that TDH has affinity for ganglioside G_{T1} (*7*). The spectral similarity between TDHi and TDH bound to lipid vesicles suggests that the latter has β-rich structures that may be similar to those of TDHi.

Inhibitory Effect of Congo Red on TDH Hemolysis. Several amyloidogenic proteins can disrupt membranes or form channels when bound to lipid vesicles (*33*, *34*). Importantly, the hemolytic activity of Alzheimer's β-amyloid (Aβ) peptides Aβ25−35 and Aβ1−42 is inhibited by the presence of Congo red (*35*).

TDH hemolysis is also inhibited by Congo red in a dose-dependent manner. The inhibitory effects of 14, 28, 56, and 114 μM Congo red on hemolysis were approximately 66, 87, 85, and >90%, respectively (Figure 5C). Our results suggest that the inhibitory effect of Congo red on the hemolytic activity of TDH may be due to the binding of this compound to the β-structures of membrane-associated TDH.

DISCUSSION

In this study, we have demonstrated that the mechanism of the Arrhenius effect on TDH originates from heat-induced conformational changes of the protein in forming fibrils. Heat-induced TDHi fibrils develop when TDH is incubated around 60 °C. TDHi fibrils are stable and do not dissociate into native TDHn without heat denaturation, even when the temperature is lowered to 4 °C (Figure 3C−E). The model of the heat-induced conformational change of TDH is summarized in Figure 7.

TDHi trapped in fibrillar structures has no hemolytic activity at 37 °C, consistent with the Arrhenius effect. The characteristics of TDHi are similar to those of amyloid fibrils in the sense that it shows an increase in thioflavin T fluorescence and enhancement of growth rate by the addition of preformed TDHi. TDHi fibrils incubated above 80 °C dissociate into unfolded states, which can refold into toxic TDHn upon rapid cooling to 37 °C. In this sense, TDH is not a heat-stable toxin, but rather a heat-reversible toxin. This is an unusual phenomenon because the formation of inactive protein aggregates is generally irreversible.

Electron and atomic force microscopic images show the remarkably diverse morphologies of amyloid fibrils. Mature amyloid fibrils typically adopt a so-called rigid needlelike

structure, with a uniform diameter of ~10 nm. Protofibrils often intertwine into left-handed helices or are laterally associated into regular periodic fibrils with a left-hand twist. However, immature β_2-microglobulin (β_2-m) fibrils are short in length and highly curved and do not appear to be composed of protofibrils (*36*). Although fibrils of disulfide-reduced β_2-m are uniform in diameter (2 nm), they are still curved, flexible, and much thinner than mature fibrils (*37*). The morphology of TDHi under the electron microscope differs from that of mature amyloid fibrils. TDHi fibrils were found to be ~10 nm in diameter, relatively short in length (<1 μm), and curvilinear like a tangled ribbon. At first glance, TDHi fibrils resemble immature amyloid fibrils of β_2-m or the fibrils of disulfide-reduced β_2-m, although the diameters of the fibrils differ significantly.

More than 20 diseases are now known to be related to the formation of amyloid fibrils by particular proteins (*29*, *35*, *38*, *39*). However, even proteins unrelated to any diseases can form amyloid fibrils in vitro, depending on the conditions (*15*−*20*). Little amino acid homology was found among amyloidogenic proteins, suggesting that amyloid formation is a generic property of the polypeptide chain. However, there are still arguments about whether the mature amyloid fibril or some other conformational state of the amyloidogenic protein is toxic (*40*). The preformed mature fibrils of proteins from the SH3 domain from bovine phosphatidylinositol 3′-kinase and the amino-terminal domain of the *E. coli* HypF protein appear to be inherently harmless to cells (*40*), which agrees with our result that heat-induced extracellularly formed TDHi fibrils displayed no hemolytic activity. It is also reported that perfringolysin O, one of the cholesterol-dependent cytolysins secreted by *Clostridium perfringens*, is required for the oligomerization into pore structures through the conformational transition around α-helical regions, in the soluble monomeric state to form intermolecular β-sheets (*41*, *42*). This finding is also consistent with our data which show that TDH forms β-rich secondary structures in the lipid environment, which is spectroscopically similar to that of heat-induced fibrillar TDHi.

The channel hypothesis of Alzheimer's disease or Huntington's disease proposes that the pathogenic amyloid peptides or polyglutamine peptides damage organs by forming ion channels. Flux studies show that TDH can induce the formation of a cation channel (*43*).

The pathological hallmark of amyloids is to bind the Congo red dye. Recent reports show that Congo red also binds to amyloidogenic peptides or proteins (i.e., Aβ1−42, Aβ25−35, prion protein, and PrP106−126) and can inhibit channel formation in vitro. However, Congo red does not block cytotoxicity once the pathogenic peptides are inserted into the membrane (*33*). We also focused on the inhibitory effect of Congo red on TDH hemolysis. Addition of Congo red inhibited the hemolytic activity of TDH, as shown previously for other amyloidogenic proteins (*33*, *35*).

Aβ adheres to the cell membrane by binding with phospholipids or ganglioside G_{M1} (*29*, *44*). The lipid-bound Aβ peptides accelerate amyloid fibril formation (*45*) and cause membrane disruption (*35*). Our data indicate that TDHi does not show any cytotoxicity against the red blood cells. On the other hand, the Congo red experiment and the observation of conformational change in lipid vesicles of TDH suggest that the protein changes its conformation in the biological membrane. Such conformational change may contribute to the membrane damage. The mechanism by which amyloidogenic proteins are sensitive to Congo red upon binding to ganglioside may be similar to that of TDH hemolysis. Thus, further investigation is needed to clarify whether the TDH aggregation or fiber formation in biological membranes is essential for its hemolytic activity.

ACKNOWLEDGMENT

We are grateful to Prof. Yuji Goto (Institute for Protein Research, Osaka University) for valuable discussions. We thank S. Nishikori and T. Nakanishi for their assistance.

REFERENCES

1. Miwatani, T., Takeda, Y., Sakurai, J., Yoshihara, A., and Taga, S. (1972) Effect of heat (Arrhenius effect) on crude hemolysin of *Vibrio parahaemolyticus*, *Infect. Immun. 6*, 1031−1033.
2. Arrhenius, S. (1907) Anwendungen der physikalischen Chemie auf die Lehre von den physiologischen Antikoerpern, *Immunochemie*, Akademische Verlagsgesellschaft, Leipzig, Germany.
3. Vasil, M. L., Liu, P. V., and Iglewski, B. H. (1976) Temperature-dependent inactivation factor of *Pseudomonas aeruginosa* exotoxin A, *Infect. Immun. 13*, 1467−1472.
4. Coolbaugh, J. C., and Williams, R. P. (1978) Production and characterization of two hemolysins of *Bacillus cereus*, *Can. J. Microbiol. 24*, 1289−1295.
5. Albesa, I., Barberis, L. I., Pajaro, M. C., Farnochi, M. C., and Eraso, A. J. (1985) A thiol-activated hemolysin in gram-negative bacteria, *Can. J. Microbiol. 31*, 297−300.
6. Iida, T., and Honda, T. (1997) Hemolysins produced by *Vibrios*, *J. Toxicol. Toxin Rev. 16*, 215−227.
7. Takeda, Y., Honda, T., and Miwatani, T. (1976) Inactivation of the biological activities of the thermostable direct hemolysin of *Vibrio parahaemolyticus* by ganglioside G_{T1}, *Infect. Immun. 14*, 1−5.
8. Honda, T., Ni, Y., and Miwatani, T. (1992) The thermostable direct hemolysin of *Vibrio* parahaemolyticus is a pore-forming toxin, *Can. J. Microbiol. 38*, 1175−1180.
9. Song, L., Hobaugh, M. R., Shustak, C., Cheley, S., Bayley, H., and Gouaux, J. E. (1996) Structure of staphylococcal α-hemolysin, a heptameric transmembrane pore, *Science 274*, 1859−1866.
10. Palmer, M., Harris, R., Freytag, C., Kehoe, M., Tranum-Jensen, J., and Bhakdi, S. (1998) Assembly mechanism of the oligomeric streptolysin O pore: The early membrane lesion is lined by a free edge of the lipid membrane and is extended gradually during oligomerization, *EMBO J. 17*, 1598−1605.
11. Gilbert, R. J. C., Jiménez, J. L., Chen, S., Tickle, I. J., Rossjohn, J., Parker, M., Andrew, P. W., and Saibil, H. R. (1999) Two structural transitions in membrane pore formation by pneumolysin, the pore-forming toxin of *Streptococcus pneumoniae*, *Cell 97*, 647−655.
12. Wallace, A. J., Stillman, T. J., Atkins, A., Jamieson, S. J., Bullough, P. A., Green, J., and Artymiuk, P. J. (2000) *E. coli* hemolysin E (HlyE, ClyA, SheA): X-ray crystal structure of the toxin and observation of membrane pores by electron microscopy, *Cell 100*, 265−276.
13. Naim, R., Yanagihara, I., Iida, T., and Honda, T. (2001) *Vibrio parahaemolyticus* thermostable direct hemolysin can induce an apoptotic cell death in Rat-1 cells from inside and outside of the cells, *FEMS Microbiol. Lett. 195*, 237−244.
14. Carrell, R. W., and Gooptu, B. (1998) Conformational changes and disease: Serpins, prions and Alzheimer's, *Curr. Opin. Struct. Biol. 8*, 799−809.
15. Chiti, F., Webster, P., Taddei, N., Clark, A., Stefani, M., Ramponi, G., and Dobson, C. M. (1999) Designing conditions for in vitro formation of amyloid protofilaments and fibrils, *Proc. Natl. Acad. Sci. U.S.A. 96*, 3590−3594.
16. Chiti, F., Taddei, N., Bucciantini, M., White, P., Ramponi, G., and Dobson, C. M. (2000) Mutational analysis of the propensity for amyloid formation by a globular protein, *EMBO J. 19*, 1441−1449.
17. Chiti, F., Bucciantini, M., Capanni, C., Taddei, N., Dobson, C. M., and Stefani, M. (2001) Solution conditions can promote

formation of either amyloid protofilaments or mature fibrils from the HypF N-terminal domain, *Protein Sci. 10*, 2541−2547.
18. Fändrich, M., Fletcher, M. A., and Dobson, C. M. (2001) Amyloid fibrils from muscle myoglobin, *Nature 410*, 165−166.
19. Guijarro, J. I., Sunde, M., Jones, J. A., Campbell, D., and Dobson, C. M. (1998) Amyloid fibril formation by an SH3 domain, *Proc. Natl. Acad. Sci. U.S.A. 95*, 4224−4228.
20. Hamada, D., and Dobson, C. M. (2002) A kinetic study of β-lactoglobulin amyloid fibril formation promoted by urea, *Protein Sci. 11*, 2411−2426.
21. Chiti, F., Stefani, M., Taddei, N., Ramponi, G., and Dobson, C. M. (2003) Rationalization of the effects of mutations on peptide and protein aggregation rates, *Nature 424*, 805−808.
22. DuBay, K. F., Pawar, A. P., Chiti, F., Zurdo, J., Dobson, C. M., and Vendruscolo, M. (2004) Prediction of the absolute aggregation rates of amyloidogenic polypeptide chains, *J. Mol. Biol. 341*, 1317−1326.
23. Kelly, J. W. (1996) Alternative conformations of amyloidogenic proteins govern their behavior, *Curr. Opin. Struct. Biol. 6*, 11−17.
24. Prusiner, S. B., Scott, M. R., DeArmond, S. J., and Cohen, F. E. (1998) Prion protein biology, *Cell 93*, 337−348.
25. Jiménez, J. L., Guijarro, J. I., Orlova, E., Zurdo, J., Dobson, C. M., Sunde, M., and Saibil, R. (1999) Cryo-electron microscopy structure of an SH3 amyloid fibril and model of the molecular packing, *EMBO J. 18*, 815−821.
26. Cohen, F. E., Pan, K. M., Huang, Z., Baldwin, M., Fletterick, R. J., and Prusiner, S. B. (1994) Structural clues to prion replication, *Science 264*, 530−531.
27. Jarrett, J. T., and Lansbury, P. T., Jr. (1993) Seeding "one-dimensional crystallization" of amyloid: A pathogenic mechanism in Alzheimer's disease and scrapie? *Cell 73*, 1055−1058.
28. Tang, G. Q., Iida, T., Yamamoto, K., and Honda, T. (1994) A mutant toxin of *Vibrio parahaemolyticus* thermostable direct hemolysin which has lost hemolytic activity but retains ability to bind to erythrocytes, *Infect. Immun. 62*, 3299−3304.
29. McLaurin, J., and Chakrabartty, A. (1996) Membrane disruption by Alzheimer β-amyloid peptides mediated through specific binding to either phospholipids or gangliosides, *J. Biol. Chem. 271*, 26482−26489.
30. Yanagihara, I., Inui, K., Dickson, G., Turner, G., Piper, T., Kaneda, Y., and Okada, S. (1996) Expression of full-length human dystrophin cDNA in mdx mouse muscle by HVJ-liposome injection, *Gene Ther. 3*, 549−553.
31. Naiki, H., Higuchi, K., Hosokawa, M., and Takeda, T. (1989) Fluorometric determination of amyloid fibrils in vitro using the fluorescent dye, thioflavin T, *Anal. Biochem. 177*, 244−249.
32. Li, S. C., and Deber, C. M. (1994) A measure of helical propensity for amino acids in membrane environments, *Nat. Struct. Biol. 1*, 368−373.
33. Kagan, B. L., Hirakura, Y., Azimov, R., Azimova, R., and Lin, M. C. (2002) The channel hypothesis of Alzheimer's disease: Current status, *Peptides 23*, 1311−1315.
34. Kourie, J. I., and Henry, C. L. (2002) Ion channel formation and membrane-linked pathologies of misfolded hydrophobic proteins: The role of dangerous unchaperoned molecules, *Clin. Exp. Pharmacol. Physiol. 29*, 741−753.
35. Mattson, M. P., Begley, J. G., Mark, R. J., and Furukawa, K. (1997) Aβ25−35 induces rapid lysis of red blood cells: Contrast with Aβ1−42 and examination of underlying mechanisms, *Brain Res. 771*, 147−153.
36. Kad, N. M., Thomson, N. H., Smith, D. P., Smith, D. A., and Radford, S. E. (2001) β_2-Microglobulin and its deamidated variant, N17D form amyloid fibrils with a range of morphologies in vitro, *J. Mol. Biol. 313*, 559−571.
37. Katou, H., Kanno, T., Hoshino, M., Hagihara, Y., Tanaka, H., Kawai, T., Hasegawa, K., Naiki, H., and Goto, Y. (2002) The role of disulfide bond in the amyloidogenic state of β_2-microglobulin studied by heteronuclear NMR, *Protein Sci. 11*, 2218−2229.
38. Tan, S. Y., and Pepys, M. B. (1994) Amyloidosis, *Histopathology 25*, 403−414.
39. Kelly, J. W. (2002) Towards an understanding of amyloidogenesis, *Nat. Struct. Biol. 9*, 323−325.
40. Bucciantini, M., Giannoni, E., Chiti, F., Baroni, F., Formigli, L., Zurdo, J., Taddei, N., Ramponi, G., Dobson, C. M., and Stefani, M. (2002) Inherent toxicity of aggregates implies a common mechanism for protein misfolding diseases, *Nature 416*, 507−511.
41. Shatursky, O., Heuck, A. P., Shepard, L. A., Rossjohn, J., Parker, M. W., Johnson, A. E., and Tweten, R. K. (1999) The mechanism of membrane insertion for a cholesterol-dependent cytolysin: A novel paradigm for pore-forming toxins, *Cell 99*, 293−299.
42. Ramachandran, R., Tweten, R. K., and Johnson, A. E. (2004) Membrane-dependent conformational changes initiate cholesterol-dependent cytolysin oligomerization and intersubunit β-strand aliment, *Nat. Struct. Mol. Biol. 11*, 697−705.
43. Lang, P. A., Kaiser, S., Myssina, S., Birka, C., Weinstock, C., Northoff, H., Wieder, T., Lang, F., and Huber, S. M. (2004) Effect of *Vibrio parahaemolyticus* haemolysin on human erythrocytes, *Cell. Microbiol. 6*, 391−400.
44. Yanagisawa, K., Osaka, A., Suzuki, N., and Ihara, Y. (1995) G_{M1} ganglioside-bound amyloid β-protein (Aβ): A possible form of preamyloid in Alzheimer's disease, *Nat. Med. 1*, 1062−1066.
45. Choo-Smith, L. P., Garzon-Rodriguez, W., Glabe, C. G., and Surewicz, W. K. (1997) Acceleration of amyloid fibril formation by specific binding of Aβ-(1−40) peptide to ganglioside-containing membrane vesicles, *J. Biol. Chem. 272*, 22987−22990.

BI050311S